Study of Titanium, Vanadium, Chromium and Manganese Doped Lead Free Double Perovskites $Cs_2NaGaBr_6$ for Potential Solar Cell Application

By

Ahmed Zabir Hussain
18311001

A thesis submitted to the Department of Mathematics and Natural Science in partial fulfillment of the requirements for the degree of
B.Sc. in Physics

Mathematics and Natural Science
Brac University
March 2024

Declaration

It is hereby declared that

1. The thesis submitted is my own original work while completing degree at Brac University.
2. The thesis does not contain material previously published or written by a third party, except where this is appropriately cited through full and accurate referencing.
3. The thesis does not contain material that has been accepted, or submitted, for any other degree or diploma at a university or other institution.
4. I have acknowledged all main sources of help.

Student's Full Name & Signature:

Ahmed Zabir Hussain
18311001

Approval

The thesis titled "Study of Titanium, Vanadium, Chromium and Manganese Doped Lead-Free Double Perovskites $Cs_2NaGaBr_6$ for Potential Solar Cell Application" submitted by Ahmed Zabir Hussain (18311001) of Summer, 2018 has been accepted as satisfactory in partial fulfillment of the requirement for the degree of B.Sc. in Physics on 25th March, 2024.

Examining Committee:

Supervisor:
(Member)

_____

Md. Firoze Haque
Associate Professor, Mathematics and Natural Science
Brac University

Co-Supervisor:
(Member)

_____

Muhammad Lutfor Rahman
Assistant Professor, Mathematics and Natural Science
Brac University

Program Coordinator:
(Member)

_____

Md. Firoze Haque
Associate Professor, Mathematics and Natural Science
Brac University

Departmental Head:
(Chair)

_____

A F M Yusuf Haider
Professor and Chairperson, Mathematics and Natural Science
Brac University

Ethics Statement

To our current understanding, this study is the first theoretical exploration showing that metal-doped double Perovskite $Cs_2NaGaBr_6$ samples are suitable for optoelectronic applications. These materials show remarkable optical absorption and conductivity properties in visible spectra.

Abstract

Lead-free inorganic double perovskites are making notable progress in the field of solar cells and optoelectronic devices. Promising materials such as $Cs_2NaGaBr_6$ are emerging as competitive alternatives. This research work studied the structural, electronic, and optical properties of pristine $Cs_2NaGaBr_6$ and Vanadium (V), Titanium (Ti), Chromium (Cr), and Manganese (Mn), doped sample, applying density functional theory for our analysis. This study is the first theoretical exploration of the doped $Cs_2NaGaBr_6$ perovskites, uncovering extraordinary results. The study reveals that all versions with added impurities show enhanced optical absorption and high optical conductivity, covering wavelengths of the visible spectrum. The wide range of performance is especially important for optoelectronic applications since it indicates greater effectiveness in absorbing solar energy. The study analyzed the electronic properties of $Cs_2NaGaBr_6$ perovskites, revealing significant changes in the band gap for each doped variation. This allows for precise tuning of the band gap, enhancing solar energy absorption. The study also found a higher density of accessible electronic states around the fermi level in doped samples, indicating increased electrical and optical conductivity. The results suggest that doping can be used to customize and enhance optical and electronic properties, creating opportunities for advanced solar cells and sustainable energy solutions.

Dedication

In humble gratitude, I dedicate this thesis to my beloved father, Md Burhan Hussain, and my cherished mother, Haifza Begum, who have selflessly sacrificed since my birth, ensuring a bright future for me.

Acknowledgment

I want to thank Almighty Allah for providing me the the resilience, bravery, and patience to finish this research.

I owe a huge debt of gratitude to my supervisors, Dr. Firoze Haque and Md Lutfor Rahman for guiding me through this project. Despite being busy, they always found time for me, answered my questions, and supported me every step of the way.

I am grateful to all the faculty members of Mathematics and Natural Science, Brac University for their constant encouragement and guidance. I am also grateful to my senior researcher Dolon Pal for his guidance and mentorship.

I would like to extend my gratitude to all of my friends and relatives. Also, I want to mention my beloved Ayesha Tahmina Hussain, Tahira Rayesa Hussain, and Irfana Arafin who have been my most supportive companions.

Finally, I want to acknowledge my incredible parents, Md. Burhan Hussain and Hafiza Begum. Their selfless sacrifices, made with unwavering love, have shaped me into who I am today. Words fail to capture the depth of my gratitude towards them.

Table of Contents

List of Tables

List of Figures

Chapter 1

Introduction

1.1 Background

Condensed matter refers to the branch of physics that deals with the physical properties of solid and liquid materials. This field extensively explores the various physical characteristics of matter in its condensed phases, including both solid and liquid forms. It plays a crucial role in comprehending the behaviors and interactions of numerous particles that strongly interact with each other. These particles can be found in various states such as solids, liquids, dense plasmas, glasses, and polymers. The main focus of condensed matter physics is to investigate the various structural, electrical, optical, and elastic characteristics that exist in both solid and liquid states. This exploration encompasses a wide range of scales, from the very small to the very large, providing a thorough understanding of the properties of materials. The field's importance is emphasized by its deep influence on several aspects of modern life, affecting a broad spectrum of modern technology and applications. Condensed matter physics is a fundamental field in the progress of scientific knowledge and technological development since it extensively investigates the characteristics of materials. When the energy of matter is sufficiently low, it must be condensed in order to form stable systems of atoms and molecules [1]. Condensed matter physics involves the use of both theoretical and experimental approaches to improve mathematical models and deepen our understanding of the physical features of the systems being investigated. Acquiring a comprehensive comprehension of condensed systems requires the use of computational or theoretical methods, which, although difficult, have become more crucial in the fields of Physics and Material Science. Recently, there has been an increased focus on calculating atomic and electronic structures, which has made it easier to determine different physical characteristics of materials using a fundamental approach. This strategy is based on quantum mechanics and depends on fundamental physical constants, providing a more direct and theoretically rigorous approach to exploration. Conversely, experimental methods, such as semi-empirical procedures, utilize empirical data to simplify calculations. Nevertheless, because of inherent constraints in semi-empirical approaches, the first-principles approach arises as a more efficient strategy for

determining various physical characteristics of solid materials. This method not only offers a more precise representation of material properties but also opens up possibilities for revolutionary progress in the comprehension of condensed matter physics.

In recent times, there has been a significant focus on the performance of photovoltaic devices using perovskite-type materials [2], [3], [4], [5], [6]. This is mostly attributed to their remarkable optical and electrical characteristics. Indeed, perovskite solar cells of commendable efficiency exhibit instability. In addition, they are constructed using lead (Pb), a substance known for its toxicity[7]. Unfortunately, this severely restricts their application in photovoltaics. In order to address this issue, researchers have proposed the use of a new class of perovskites known as double perovskites [8], [9]. The suggested compounds are inorganic, stable, non-toxic, and have been effectively synthesized [8], [9], [10], [11]. These characteristics make them highly suitable for photovoltaic applications. The analysis of mechanical properties given in a theoretical work [12] discloses a bandgap of 1.762 eV computed with SOC + mBJ for $Cs_2NaGaBr_6$, which is similar to the parent organic–inorganic perovskite $CH_3NH_3PbI_3$ (E_g = 1.6 eV). In the present experiment, the observed bandgap of 1.423 eV is computed using the GGA, PBE method for $Cs_2NaGaBr_6$. In order to increase the optical absorbance in the visible light energy region, it is necessary to find a suitable dopant for $Cs_2NaGaBr_6$ to tune the bandgap. Hence, the objective of this study is to introduce different transition metals into the Ga-site of $Cs_2NaGaBr_6$ in order to increase the optical absorbance throughout the entire range of the solar spectrum.

1.2 Objectives of the Research

The primary objective of this research is to thoroughly investigate the physical properties of pure and transition metal-doped $Cs_2NaGaBr_6$, with a specific focus on improving the efficiency of optoelectronic devices.

DFT is employed to perform the following tasks:

- Examination of the structural characteristics of original and transition metal-infused $Cs_2NaGaBr_6$.
- Exploration into the electronic attributes (band structure and density of states) of both the unadulterated and metal-doped specimens.

- Analysis of the optical traits (Absorption, Conductivity, Reflectivity, and Dielectric constant) of the untainted and modified $Cs_2NaGaBr_6$.

1.3 Outline of the Thesis

The subsequent sections of the thesis are organized as follows:

- **Chapter 2**: This chapter presents a comprehensive review of the existing literature, coupled with an in-depth theoretical analysis of the properties under investigation.
- **Chapter 3**: This chapter is dedicated to detailing the fundamental theoretical approaches, particularly emphasizing the first-principles calculations employed in the study.
- **Chapter 4**: This chapter includes the results and a thorough discussion, investigating various physical properties examined as part of this research.
- **Chapter 5**: The final chapter offers a conclusion, reflections on the research findings, and an overview of prospective future directions and applications.

Chapter 2

Literature Review and Theoretical Background of Investigated Properties

2.1 Literature Review

In recent years, double perovskites have emerged as a focal point in the field of optoelectronics, largely driven by their potential as alternatives to conventional perovskite materials [8], [9]. These materials are stable, inorganic, nontoxic, and synthesized [8], [9], [10], [11], making them highly suitable candidates for photovoltaic applications [13]. $Cs_2NaGaBr_6$ is a type of double perovskite material that has received significant attention in recent years. It has been suggested as a highly promising option for various technological applications, particularly in the field of photovoltaics [12], [14]. From the study of Saeed et al., the computed bandgap of $Cs_2NaGaBr_6$ is reported to be 1.762 eV [12]. Another study by Kumar et al. shows the enhancement of $Cs_2NaGaBr_6$ solar cells by ETL optimizations, where they reported a higher efficiency of 25.86% with optimized doping concentration of the electron transport layer (ETL) [14]. In past years, metal-doped perovskites have given promising results, particularly in enhancing their optoelectronic properties [15], [16], [17]. This present study aims to investigate the impact of similar doping strategies on the performance of double perovskite materials. Hence, this study focuses on thoroughly examining the structural, electronic, and optical properties of $Cs_2NaGaBr_6$ samples doped with Ti, V, Cr, and Mn. The investigation utilizes Density Functional Theory (DFT) to identify a better lead-free metal halide double perovskite that can enhance the performance of optoelectronic devices. A comprehensive comparison is presented, examining the distinct characteristics of pristine and metal-doped $Cs_2NaGaBr_6$.

2.2 Fundamental Aspects of Crystal

The crystal structure of a material is a critical determinant of its properties, defined by the periodic arrangement of its constituent atoms, ions, or molecules. The periodicity of a crystal is vital to its physical properties, exerting an impact on its mechanical, elastic, and optical properties. Materials

can be generically classified into crystalline and amorphous, depending on the arrangement of their atoms. Crystalline materials, such as Barium chloride ($BaCl_2$) and Silicon dioxide (SiO_2), exhibit a well-defined and uniform microscopic arrangement. Conversely, amorphous materials, such as Polyvinyl chloride and Fiber-glass, lack such periodicity, leading to fundamentally different characteristics. Several materials, such as certain ceramics and geological formations, are polycrystalline, meaning they consist of several crystalline grains with different sizes and orientations. The structure of a crystal is determined by the interaction between its lattice and basis. A lattice is a structured arrangement of points that determines the geometric order of a crystal. Each lattice point is typically occupied by a basis, which consists of a set of atoms or molecules. The foundation is crucial in determining the structure, configuration, and alignment of the atoms within the crystal. This chapter explores the crystal structure and several structural characteristics of the $Cs_2NaGaBr_6$ perovskite-type semiconductor. $Cs_2NaGaBr_6$, a double perovskite, possesses a complex lattice arrangement that greatly impacts its electronic, optical, and structural properties. The unique optoelectronic features of this material are a result of its unique arrangement of cesium, sodium, gallium, and bromine atoms, which makes it suitable for advanced semiconductor applications.

In-depth analysis of these features is conducted using advanced computational approaches, such as Density Functional Theory (DFT). These theoretical frameworks enable precise modeling of the crystal's behavior under various conditions, providing an in-depth understanding of its possible uses. The objective of this chapter is to offer a detailed comprehension of the crystal structure of $Cs_2NaGaBr_6$, emphasizing its significance in the field of semiconductor research and its practical applications. The investigation encompasses theoretical models employed in the study of the material's structural, electronic, and optical properties, highlighting its importance in the realm of sophisticated optoelectronic devices.

2.3 Crystal Structure of $Cs_2NaGaBr_6$

2.3.1 Unit cell

The $Cs_2NaGaBr_6$ forms a crystalline structure that belongs to the cubic perovskite-type group, which is with the space group $Fm\bar{3}m$. The crystal structure of $Cs_2NaGaBr_6$ is drawn by the

software VESTA (Visualization for Electronic and Structural Analysis). The visualization is shown in Figure 2.1. The crystal's unit cell contains ten atoms in a single formula unit. The Cs atoms are located at the center and occupy the 2c Wyckoff position, Na atoms are located at the body-centered site with the 1b Wyckoff position, Ga atoms are also located at the body-centered positions and occupy the 1a Wyckoff position and the Br atoms take place at the face-centered position [18].

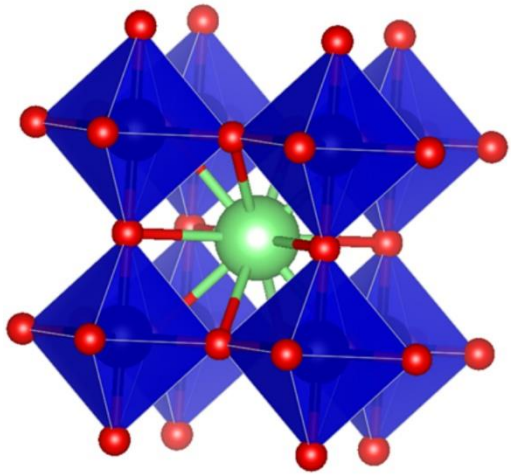

Fig. 2.1: Crystal structure of $Cs_2NaGaBr_6$ (unit cell).

2.3.2 Lattice parameters

The lattice parameters refer to the lengths of the cell edges along each crystallographic axis. The parameters refer to the dimensions of the unit cell edges, denoted as a, b, and c, which align with the crystallographic axes. In addition, the unit cell is determined by the angles created by the intersection of its edges. Specifically, α represents the angle opposite edge a, which is generated by the intersection of edges b and c; β represents the angle opposite edge b, formed by the intersection of edges c and a; and γ represents the angle opposite edge c, formed by the intersection of edges a and b. These parameters define both the dimensions and configuration of the unit cell and also enable the calculation of the distances between neighboring atoms in the crystal structure, which is crucial for understanding its properties. The relationship among the lattice parameters of $Cs_2NaGaBr_6$ is $a = b = c = 10.09$ Å and $\alpha = \beta = \gamma = 90°$ [18].

2.3.3 Volume of the unit cell

The vectors a, b, and c represent the lengths of the cell edges, while α, β, and γ represent the inter-axial angles.

Here, Volume of the unit cell, $V = \boldsymbol{a} \cdot (\boldsymbol{b} \times \boldsymbol{c})$.

Now, $V = abc\,[\sqrt{}\,(1 - cos2\alpha - \cos2\,\beta - \cos2\,\gamma + 2cos\alpha cos\beta cos\gamma)]$ (2.1)

$$V = a^3 \quad (2.2)$$

By putting the value of a of the cubic crystal $Cs_2NaGaBr_6$, the volume, V = 1027.24 Å^3. (2.3)

2.4 First-Principles Computational Details

The ab initio Density Functional Theory (DFT) simulations were conducted using the plane wave pseudopotential method implemented in the CASTEP (Cambridge Serial Total Energy Package) module of Materials Studio [19]. The electron-ion interaction was described using a Vanderbilt-type ultrasoft pseudopotential [20]. The improved version of PBE (Perdew-Berke-Ernzerhof) [21] utilized GGA (Generalized Gradient Approximation) to calculate the exchange-correlation energy. Calculations involving pseudo-atomic models are performed by taking into account the valence electrons. An investigation was conducted to examine the impact of doping on $Cs_2NaGaBr_6$. This was achieved by creating a 1× 1 ×1 supercell, which consisting of 40 atoms. Consequently, the $Cs_2NaGaBr_6$ material is modified with metal doping, resulting in a new chemical formula $Cs_2NaGa_{1-x}M_xBr_6$ (x = 0.25 and M = Ti, V, Cr, Mn). The energy cutoff for the plane wave is 500 eV, and it is used in conjunction with k-points 3×3×3. Both the geometric optimization and electronic properties study were conducted using the supercells of pure and doped metal halide perovskites. The Monkhorst-pack method [22] was employed to sample the k-points. The L-BFGS technique [23] was used to get the most efficient arrangement in the crystal structure. The convergence thresholds are:

(i) Total energy: 1.000×10^{-5} eV/atom

(ii) Maximum stress: 5.000×10^{-2} GPa

(iii) Maximum force: 3.000×10^{-2} eV/Å

(iv) Maximum displacements: 1.000×10^{-3} Å.

2.4.1 Geometry optimization

Geometry optimization plays a vital role in CASTEP computations as it enables the identification of the molecule's configuration with the lowest energy. This process is crucial as it has a significant impact on numerous physical and chemical properties of the molecule. The primary emphasis in computational chemistry is to optimize the molecular geometry. The objective of this optimization is to identify the minima on the potential energy surface, which corresponds to the equilibrium configurations of the molecule. Furthermore, optimization techniques are utilized to detect transition structures, which are depicted as saddle points on this surface. Energy minimization, also known as molecular energy reduction, is the act of altering atomic coordinates to decrease the overall energy of a molecule. Energy minimization is an essential prerequisite in both molecular mechanics and quantum mechanics approaches, and it must be carried out before performing any computational analysis utilizing these methods.

Chapter 3

Theoretical Methodology

3.1 Classification of Methodology

Recently, researchers have shown significant interest in using computer-based theoretical calculations to investigate material properties in the fields of natural science. Occasionally, it is beneficial to carry out computer-based theoretical computations that are more reliant on mathematical models and equations rather than analytical investigations. Multiple techniques are used to analyze the structure and discover the diverse characteristics of the substance. The approaches can be categorized by 3 distinct types:

(i) First-principles or ab initio.
(ii) Empirical or semi-empirical.
(iii) Molecular mechanics.

First-concepts or ab initio approaches rely solely on theoretical principles and do not rely on empirical data for the computations. The ab initio approaches heavily rely on the principles of quantum physics and the precise values of a limited number of physical constants. Ab initio approaches can yield highly precise findings for calculating tiny molecular systems, and efforts are underway to expand their applicability to larger molecule systems. Semi-empirical approaches rely on empirically obtained empirical data to simplify calculations. While these methods are capable of doing calculations for big molecules, their accuracy is somewhat reduced. Molecular mechanics approaches employ classical physics to investigate the dynamics of atoms and molecules. The majority of the procedures given in this chapter are the first method. These approaches are valuable for anticipating the properties of novel materials, such as calculating the energy levels of electrons in solids. This calculation helps determine the energy bands, which is a fundamental theoretical challenge in solid-state physics. Previously, ab initio approaches were significantly constrained in their practical applicability to systems of restricted size. However, both of these approaches have consistently faced the issue that, in the absence of computer assistance,

they are not feasible for actual systems because of the extensive amount of integrals that need to be calculated. Currently, with the significant advancement of affordable, high-performance computers, it is practical to accurately study the energies and associated characteristics of systems consisting of a small number of atoms, including the heaviest elements in the periodic table. This analysis takes into account relativistic effects and can be completed in just a few minutes on a standard workstation. Unlike other methods, ab initio calculations have the ability to produce accurate quantitative predictions for a wide range of systems. Hence, in this study, the simulation were conducted using an ab initio plane-wave pseudopotential approach inside the DFT framework, employing GGA as implemented in the CASTEP tool [19]. The purpose was to examine the optical, structural, and electrical properties.

3.2 Wave Function

A wave function is a mathematical function that characterizes the likelihood of finding a particle in a certain quantum state, taking into account its position, time, momentum, and/or spin. The symbol ψ is commonly used to represent wave functions. The wave function is a fundamental concept employed in the field of quantum mechanics. As a mathematical technique, it is used to describe the quantum state. The wave function is a mathematical function that solves the wave equation and describes the characteristics of a wave. A wave function is represented by the notation $|\psi|^2$. The chance of locating the particle at a specific time and position is determined by the magnitude of the wave function, $|\psi|^2$. The principles of quantum physics, namely the Schrödinger equation, delineate the temporal evolution of the wave function. The wave function exhibits similar qualitative behavior to other types of waves, such as water waves or waves on a string, due to the mathematical nature of the Schrödinger equation, which is a form of wave equation. This explains the term "wave function" and its connection to the concept of wave-particle duality. The wave function's evolution over time, as governed by the Schrödinger equation, also encapsulates the dynamic behavior of quantum systems, offering insights into their temporal changes and interactions with their environment.

3.3 The Schrödinger Equation

The Schrödinger equation is the fundamental equation in Physics used to investigate the quantum mechanical system. The Schrödinger wave equation, often known as a partial differential equation, describes the evolution of the wave function of a quantum system. The Schrödinger equation is utilized to derive the allowed energy states of quantum mechanical systems. The name "Schrödinger equation" refers to two separate equations, often known as the time-dependent and time-independent Schrödinger equation.

$$\hat{H}\psi = E\psi \tag{3.1}$$

Here, $\hat{H}$ is the Hamiltonian that acts on the wavefunction ψ and gets E, which represents the entire energy of the system. More operators can be utilized, such as spin and electric dipole moments. The wave function can be utilized to derive expectation values of physical observables. The Schrödinger equation may seem relatively straightforward to solve, but in actuality, it is unsolvable without making approximations for non-hydrogenic systems. The Born-Oppenheimer (BO) approximation is the most fundamental approximation in which the motion of the nuclei in the system is decoupled from the motion of the electrons. The Born-Oppenheimer approximation suggests that any alteration in the positions of the atomic nuclei results in an instant reorganization of the electronic arrangement. In other words, the nuclei are considered immobile at each geometric configuration in relation to the movement of the electrons, allowing for a more convenient assessment of the interactions between the electrons and nuclei, as well as the nuclear kinetic energy. The approximation can be understood by considering the significant disparity in mass between electrons and nuclei, which causes the electrons to rapidly readjust their positions when the nuclei are in motion. The Born-Oppenheimer (BO) approximation is a relatively gentle approximation when compared to others. Working without it is only necessary in rare circumstances.

$$(H_{el} + V_N)\,\psi = E_{el}\psi_{el} \tag{3.2}$$

$$H_{el} = T_s + V_{en} + V_{es} \tag{3.3}$$

The operators in the electronic Schrödinger equation (3.2) include the electronic interactions, denoted as H_{el}, and the nuclear-nuclear interactions, denoted as V_N. In equation (3.3), "H_{el}"

represents the total energy of the system, which includes the kinetic energy of the electrons (T_e), the potential energy between the electrons and the nucleus (V_{en}), and the potential energy between the electrons themselves (V_{es}). The vibrational number (V_N) remains constant for each geometry in accordance with the Born-Oppenheimer approximation. Therefore, it can be eliminated from the equation and included as a parameter. Most quantum chemistry codes solve the electronic Schrödinger equation.

3.5 Ab initio Methods

The ab initio method is a theoretical approach that allows for the calculation of molecular structures and other properties of a crystal without relying on empirical data. Instead, this method utilizes the values of fundamental constants and the atomic numbers of the atoms involved. The term "ab initio" is derived from the Latin words "ab" (from) and "initio" (beginning). It means "from the beginning" in Latin. Ab initio calculations necessitate a substantial quantity of numerical computations, and the computational time escalates fast as the atom or molecule's size expands. The advancement in computing power has facilitated accurate calculations of the characteristics of both tiny and big molecules, rendering the semi-empirical method obsolete. Ab initio calculations are employed to determine the bond lengths and bond angles of compounds. This is done by calculating the total energy of the molecule for several molecular geometries and identifying the conformation with the lowest energy. When the magnitudes of approximations are sufficiently modest, ab initio approaches provide the advantage of being able to converge to the precise solution. The convergence, however, is non-monotonic, meaning it does not consistently increase or decrease. In many cases, the smallest calculation yields the most optimal solution for specific features. The ab initio method is used to accurately identify the physical and chemical properties of a periodic system, based on its specific chemical composition and crystalline structure. This method does not require any prior knowledge or assumptions [28].

The two widely used methods are:

i. Hartree-Fock.
ii. DFT (Density Function Theory).

We are going to describe the DFT method below.

3.5.1 Density Function Theory

The DFT was developed by Hohenberg and Kohn [29]and Kohn and Sham [30]. Density Functional Theory (DFT) is an exceptionally effective framework for characterizing the fundamental state characteristics of metals, semiconductors, and insulators. The fundamental concept behind the DFT is to describe the behavior of a system of interacting electrons based on its density rather than its many-body wave function. The DFT approach serves as a replacement for the ab initio procedure. This quantum mechanical theory explains the electronic structure, which is the lowest energy state of systems that consists of multiple particles. It is commonly used to study atoms, molecules, and condensed phases, and focuses on the distribution of electrons in space. Unlike the many body wave function, the primary concept of Density Functional Theory (DFT) is to characterize a system of interacting fermions based on its electron. Density functional theory (DFT) relies on two theorems established by Hohenberg and Kohn in 1964 [29] as well as a computational approach introduced by Kohn and Sham (KS) in subsequent years [30] They demonstrated that the overall energy is dependent on the electron density, eliminating the requirement for knowledge of the intricate many-electron wave function. Instead, only the electron density $\rho(\boldsymbol{r})$ is required, which is the fundamental quantity in Density Functional Theory (DFT).

- Theorem 1 (Uniqueness): The anticipated value of every observable in the ground state is solely determined by the exact electron density $\rho(\boldsymbol{r})$. Therefore, if the electron density and functions are known in the ground state, it is feasible to compute all the characteristics of the system. Specifically, it is feasible to compute the energy of the lowest energy state, denoted as E_0 [ρ_0].
- Theorem 2 (Variational principle): $\rho(\boldsymbol{r})$ is the solution that minimizes the total energy functional $E[\rho]$. The second theorem determines the values of $\rho_0(\boldsymbol{r})$ and $E_0[\rho]$ simultaneously using variational criterion, a set of nuclear charge give an external potential, $V(r) = -\sum_{i,j=1}^{N_{el}} \frac{z_j}{|r_j - R_j|}$

And,

$$E[\rho(\boldsymbol{r})] = E_{ext} + E_j + E_{kxc} + ER_{ep}N_{uc} \quad (3.4)$$

the self-consistent field (SCF) is used to determine the ground state energy in the Kohn and Sham (KS) method [39]. The procedures are described below:

1. The n/2 smallest eigenvalues along with their eigenfunctions are determined for the one-electron Hamiltonian:

$$\hat{h}_{eff}\psi_i(\boldsymbol{r}) = \varepsilon_i\psi_i(\boldsymbol{r}) \tag{3.5}$$

2. The density, $\rho(\boldsymbol{r})$:

$$f(x) = 2\sum_i|\psi_i(r)|^2 \tag{3.6}$$

3. The calculation of the effective volume, $Veff$, as a function of the density, $\rho(\boldsymbol{r})$:

$$V_{eff} = V(r) + \int \frac{\rho(r\prime)}{|r-r\prime|}\, dr' + \mu_{xc}(r;[\rho]) \tag{3.7}$$

   Here, exchange-correlation potential = $\mu_{xc}(r;[\rho])$

4. If a state of self-consistency is not achieved, proceed to step 1.
5. At a state of self-consistency, the density $\rho(r)$ is equal to the ground state density $\rho 0(r)$, and the energy of the ground state may be determined using equation (3.4),

$$E_0 = E_{kps} + \int \rho_0(\boldsymbol{r})\, V(\boldsymbol{r})\, d\boldsymbol{r} + 1/2 \int \frac{\rho_o(r)\rho_o(r)}{|r-r|} d\boldsymbol{r} d\boldsymbol{r}' + E_{xc} + E_{RepNu} \tag{3.8}$$

6. The utilization of the DFT approach has emerged as a potent methodology for investigating the electrical configuration of crystals. Given the intricate nature of the correlation and exchange energy formulas, their practical implementation necessitates the execution of numerical integrations. The integrals have a highly uneven spatial distribution, characterized by pronounced cusps that align with the positions of the nuclei. These integrals are computed using the analytic functions of the electron's density and its derivatives. The contribution of the electron-electron interaction to the energy must be correctly computed by the following integration:

$$E^{DFT} = \int \varepsilon^{DFT}(r)dr \tag{3.9}$$

   Here, ε^{DFT} represents the energy density of the DFT, which corresponds to the XC interaction. The parameters of a system consisting of electrons and ions are determined by computing the ground state energy using equation (3.8) based on the electron density.

3.5.1.1 Generalized Gradient Approximation

GGA offers significant enhancements in predicting the ground state characteristics of light atoms, molecules, and solids. Typically, GGA predicts larger equilibrium lattice parameters when compared to the local density approximation (LDA). The Generalized Gradient Approximation (GGA) for the exchange function, coupled with precise expressions for the correlation function, has found widespread application across various domains. Within these applications, Density Functional Theory (DFT) has excelled in providing precise structures, bond energies, and activation energies for reactions, aligning closely with meticulous ab initio computations and experimental findings. In this study, the calculations utilized the GGA approach, known for its computational efficiency relative to LDA. While LDA assumes uniformity in electron distribution, GGA addresses deviations arising from non-uniform charge densities by incorporating the charge density gradient. This refinement proves particularly advantageous for systems with slowly fluctuating charge densities or non-uniform electron distributions. As a result, GGA delivers more precise outcomes, with the E_{xc} being contingent upon the spin density and its gradients[32]:

$$E_{xc}^{GGA}[\rho\uparrow,\rho\downarrow] = \int[\rho\uparrow(r),\rho\downarrow(r),\nabla\rho\uparrow(r),\nabla\rho\downarrow(r)]\,dr \tag{3.13}$$

The implementation of GGA aims to greatly enhance the quality of LDA outcomes. The LDA method is not effective in cases when there are rapid variations in density, such as in molecules. To address this issue, the GGA method can be taken into account.

3.6 CASTEP Computer Code

CASTEP is a computational software that utilizes Density Functional Theory (DFT) and a plane wave basis set to do first principles calculations and determine various properties of materials. CASTEP was initially developed by Prof. M.C. Payne and subsequently enhanced by multiple researchers in the UK [19]. CASTEP was developed by the Theory of Condensed Matter (TCM) group during the late 1980s and early 1990s. CASTEP was originally a serial academic software developed using Fortran-77. The code underwent a complete modification from 1999-2001, utilizing Fortran-95 and MPI. This was done to take advantage of the advanced features of modern Fortran and enhance the long-term viability of the software on parallel computers. The modifications were carried out by researchers from the universities of Cambridge, York, Durham,

St. Andrews, and Rutherford labs. Due to the innovative code design, modern techniques and technologies may be easily and efficiently included in the CASTEP code. The code has been specifically developed for parallel computers, enabling the handling of significantly larger problems. The methodology for electronic structure computations performed in CASTEP can be summarized as follows: The plane-wave pseudopotential technique [20] is utilized to solve a collection of one-electron Schrödinger equations. The wavefunctions are expanded using a basis set of plane waves, which is defined by using periodic boundary conditions and Bloch's Theorem.

The modern plane-wave code is characterized by its parallel structure, ensuring efficient execution across multiple processors. The design prioritizes portability, enabling effortless adaption and utilization across various computing systems. The code is advanced, integrating the most recent advancements in computational techniques. The modular structure of the system improves its usability and maintainability, making it easier to update and modify. Furthermore, it maintains or exceeds the range of features found in the original FORTRAN 77 (F77) code, guaranteeing the preservation or improvement of all previously existing functionalities. Moreover, it preserves and enhances the functionalities of the original F77 code, incorporating developments in processing capacity and algorithms.

CASTEP is a computer program designed for first principles study, aiming to determine system physical properties through ab-initio calculations. Its basic principle is total energy calculation, which is used to derive forces and stresses. These calculations are then used for full geometry optimizations and possibly finite temperature molecular dynamics. Symmetry and constraints can be imposed in calculations, either manually or automatically using in-built detection. CASTEP can be used in serial or parallel running and uses freeform file format, requiring specific commands for computations.

The capabilities of the CASTEP code offers a wide range of computational materials science functions, which are discussed below:

- The CASTEP software accurately calculates total energy, forces, and stresses. Having this fundamental capability is crucial for understanding the stability and mechanical characteristics of materials.

- The method is highly proficient at computing and evaluating electronic structures. The analysis includes the calculation of orbitals, electronic charge densities, overall and partial electronic density of states (DOS), and band structures. Furthermore, it offers valuable information regarding optical characteristics like as absorption, reflectivity, refractive index, and dielectric function, based on the estimations of the band gap using the standard density functional theory (DFT).
- Geometry optimization involves the ability of CASTEP to optimize the placements of atoms and the characteristics of the unit cell. The optimization process can be either constrained or unconstrained, absorbing external pressure and stress. These optimizations are crucial for accurately forecasting the most stable structure of materials under different conditions.
- The software excels at identifying transition states, which are essential for understanding reaction processes and pathways in materials.
- The software provides support for different exchange and correlation functionals, such as the Local Density Approximation (LDA) and Generalized Gradient Approximation (GGA) functionals like PW91 and PBE. In addition to this, CASTEP also provides sophisticated non-local functionals, such as the weighted density approximation and Hartree-Fock (HF) exact/screened exchange, which allow for flexible management of electronic interactions.
- CASTEP performs molecular dynamics simulations at finite temperatures across many circumstances. These simulations encompass constant temperature, pressure, volume, and energy conditions, facilitating an in-depth investigation into the behavior of materials in various thermodynamic conditions.

CASTEP is a powerful and flexible tool that has a diverse range of functions necessary for better analysis and prediction of material properties.

Chapter 4

Results and Discussion

4.1 Physical Properties of Pristine and Metal-Doped $Cs_2NaGaBr_6$

4.1.1 Structural Property

We plan to study the structure of metal-doped double perovskite $A_2^{1+}B^{2+}B^{3+}X_6^{1-}$ where A_2^{1+} = Cs, B^{2+} = Na, B^{3+} = Ga, and X_6^{1-} = Br. $Cs_2NaGaBr_6$ is a three-dimensional double perovskite that crystallizes in the cubic Fm-3m space [18]. From the fig. 4.1, we can see twelve equivalent Br1- atoms and one Cs1+ produce $CsBr_{12}$ cuboctahedra. These cuboctahedra share six equivalent $CsBr_{12}$ cuboctahedra on their faces, four equivalent $NaBr_6$ octahedra on their faces, and four equivalent GaBr6 octahedra on their corners. The constructed supercell (1× 1 ×1) of $Cs_2NaGaBr_6$ contains 8 Cs atoms, 4 Na atoms, 4 Ga atoms, and 24 Br atoms as shown in the Figure.

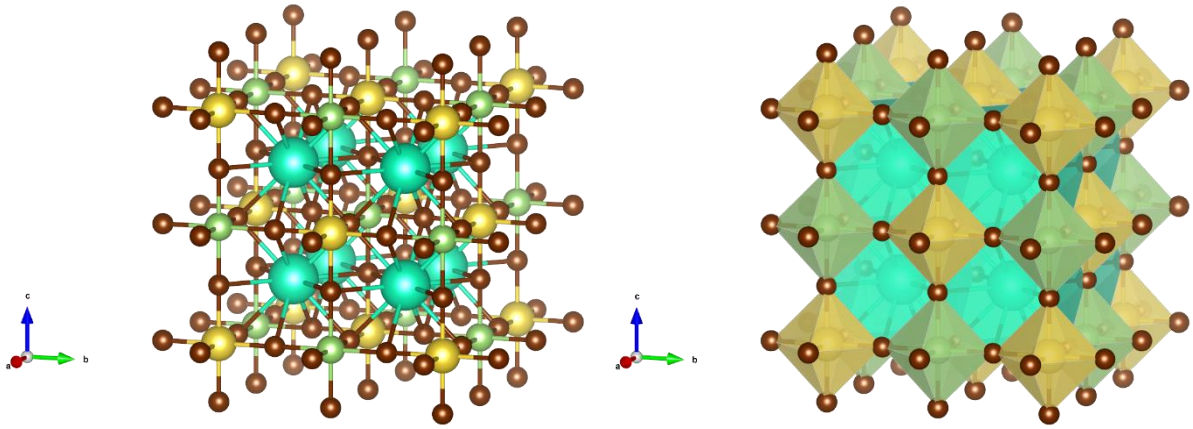

Fig. 4.1: The constructed supercell (1× 1 ×1) of $Cs_2NaGaBr_6$ double perovskite.

By substituting one Ga atom with Ti, V, Cr, and Mn, an impurity is added to the pure supercell of $Cs_2NaGaBr_6$, resulting in a doping concentration of 25%. The calculated lattice parameter for the pristine double perovskite sample is 11.1390 Å and the unit cell Volume is 1382.13 $Å^3$. These observed values are relatively close to other experimental work [12]. The calculated values also reflect consistency with experimentally synthesized double perovskites such as $Cs_2AgBiBr_6$(11.2711 Å and 1431.86$Å^3$) and $Cs_2AgBiCl_6$(10.7774Å and 1251.82$Å^3$) [33]. However, fig. 4.2 shows the doping of Ti and V exhibited higher values of lattice parameter

(11.1875Å and 11.1580 Å) and unit cell volume (1389.21Å^{3}and 1400.26Å^3) compared to the pristine sample.

Table 4.1: Optimized structural parameters of pristine and doped double perovskites.

	Optimized lattice constant (Å)	Volume (Å^3)
$Cs_2NaGaBr_6$	11.1390	1382.13
$Cs_2NaGa_{1-x}Ti_xBr_6$	11.1875	1400.26
$Cs_2NaGa_{1-x}V_xBr_6$	11.1580	1389.21
$Cs_2NaGa_{1-x}Cr_xBr_6$	11.1094	1371.08
$Cs_2NaGa_{1-x}Mn_xBr_6$	11.1031	1368.78

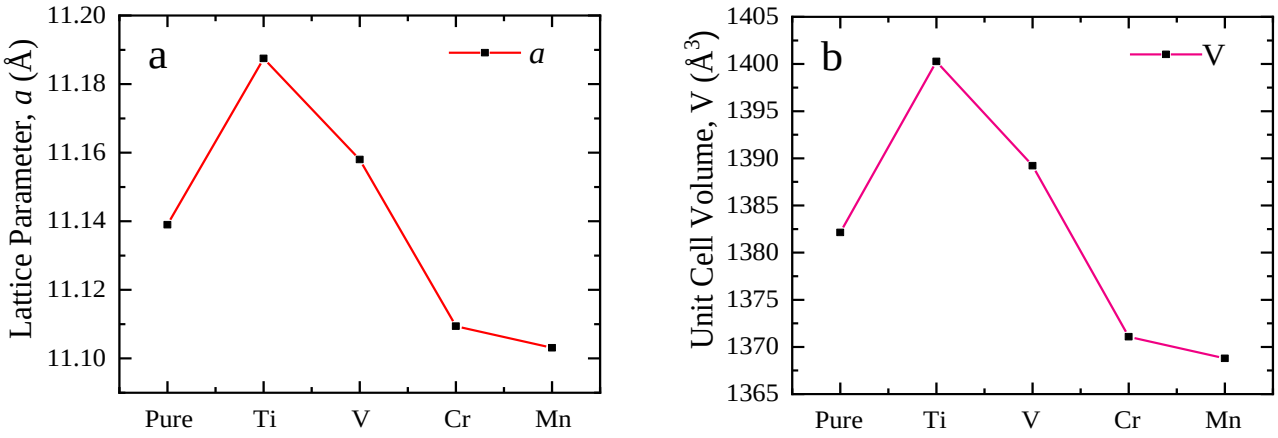

Figure 4.2: Variation of Lattice Parameter (a) and Unit Cell Volume (b) of pristine and doped concentrations of $Cs_2NaGaBr_6$.

4.1.2 Electronic Properties

In the context of the pristine and doped $Cs_2NaGaBr_6$, understanding the electronic phenomena such as band structure and Density of States (DOS) is essential for predicting and tailoring properties for specific applications, such as solar cells. In order to properly understand the optical property, the Bang structure and DOS are essential. The band structure of a material represents the ranges of energy that electrons within the material can have. The structure of the band provides insights into the material's electrical conductivity, optical properties, and how it interacts with electromagnetic fields. On the other hand, the DOS in a material describes the number of different states at each energy level that electrons are allowed to occupy. The total DOS is the sum of the density of states for all the electrons in the system. In contrast, the partial DOS provides this information for specific types of orbitals (like s, p, d) or elements in a compound, offering more detailed insight into the electronic structure.

Fig. 4.3 and Fig. 4.4 in the study show the band structures of pristine and metal-doped $Cs_2NaGaBr_6$. In these diagrams, the Fermi level (E_f), which is a crucial energy level in the material, is set at the zero point on a photon energy scale that ranges from -3 eV to +3 eV. In all the samples, the E_f is positioned between the conduction band (higher energy levels) and the valence band (lower energy levels). The behaviour of solid materials is greatly influenced by the arrangement of energy levels near the E_f. Because of this, the study focuses on examining the lower part of the conduction band and the top part of the valence band, which are close to the E_f. The band structure of pristine $Cs_2NaGaBr_6$ double perovskite is displayed in Fig. 4.3. Here, the lower point of the conduction band and the peak point of the valence band are located in the G point. As a result, the pristine $Cs_2NaGaBr_6$ exhibits a direct bandgap which makes it a semiconducting material. The observed band gap at the G symmetry point E_g = 1.423 eV. A band gap of pristine $Cs_2NaGaBr_6$ calculated with mBJ + SOC by Yasir Saeed et al. is reported to be 1.762 eV [12]. The calculation of this study was done with GGA PBE. It is clear that the GGA method underestimates the band gap value. The GGA method, frequently utilized in computational material science, often encounters limitations due to its approach to electron correlation and exchange. This is evident in the consistent underestimation of band gaps, a problem that also occurs in the LDA and LDA+U techniques. To address this issue, researchers have introduced methods like the hybrid functional [34] and the GW method [35]. However, these too have their own set of constraints. The GGA+U [36] method has been employed to partially rectify the discrepancy between theoretical and experimental band gap values. Importantly, despite these challenges, the GGA method remains

Effective for comparative studies of band structures and density of states (DOS) in pure and metal-doped $Cs_2NaGaBr_6$.

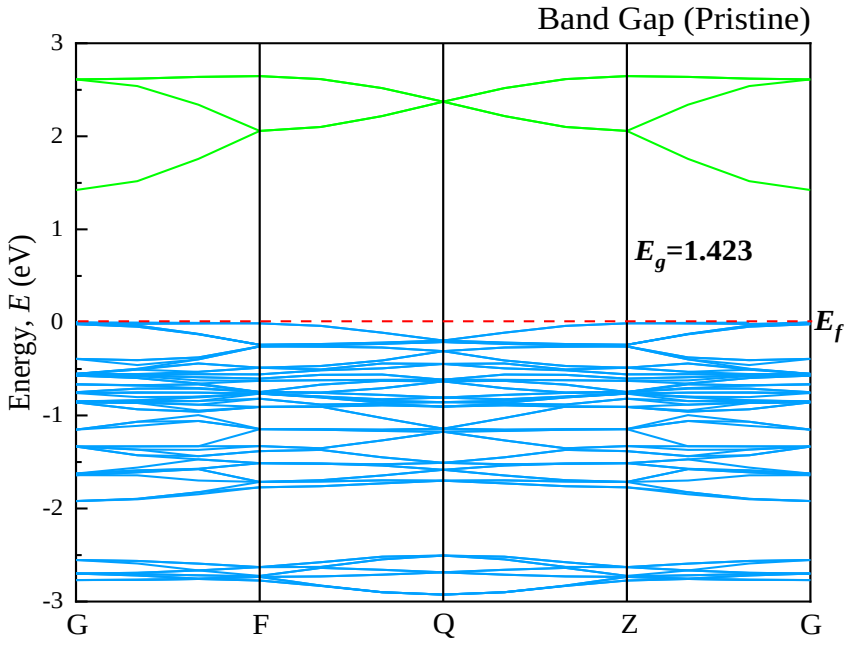

Fig. 4.3: The electronic band structure of pristine $Cs_2NaGaBr_6$ double perovskite.

Fig 4.4 demonstrates the band structures of metal-doped $Cs_2NaGaBr_6$ samples. In Fig 4.4(a), the band gap between the minimum of conduction band at the G symmetry point and the peak valence band at the G symmetry point is 1.57 eV. This results in a direct band gap and an intermediate state is also noticed near the fermi level. For the Ti-doped sample, the conduction band shifts towards the lower energy region and crosses the fermi level. Consequently, the Ti-doped sample exhibits the highest absorption in the visible region (fig. 4.7) compared to the pristine and other doped samples. Fig. 4.4(b) illustrates the band structure of V-doped $Cs_2NaGaBr_6$. Here, the band gap between the lower portion of the conduction band (at G-point) and the peak of the valence band (at G-point) is 1.62 eV (direct band-gap) which is larger than the band gap of pristine and V-doped $Cs_2NaGaBr_6$. However, due to the appearance of an intermediate state between the band gap, the band gap between the lower portion of the conduction band at G-point and the intermediate state is 0.034 eV. This intermediate state eases the transfer of electrons from the valence band to

the conduction band. Fig. 4.4(c) and Fig. 4.4(d) show the band structure of Cr-doped and Mn-doped samples respectively.

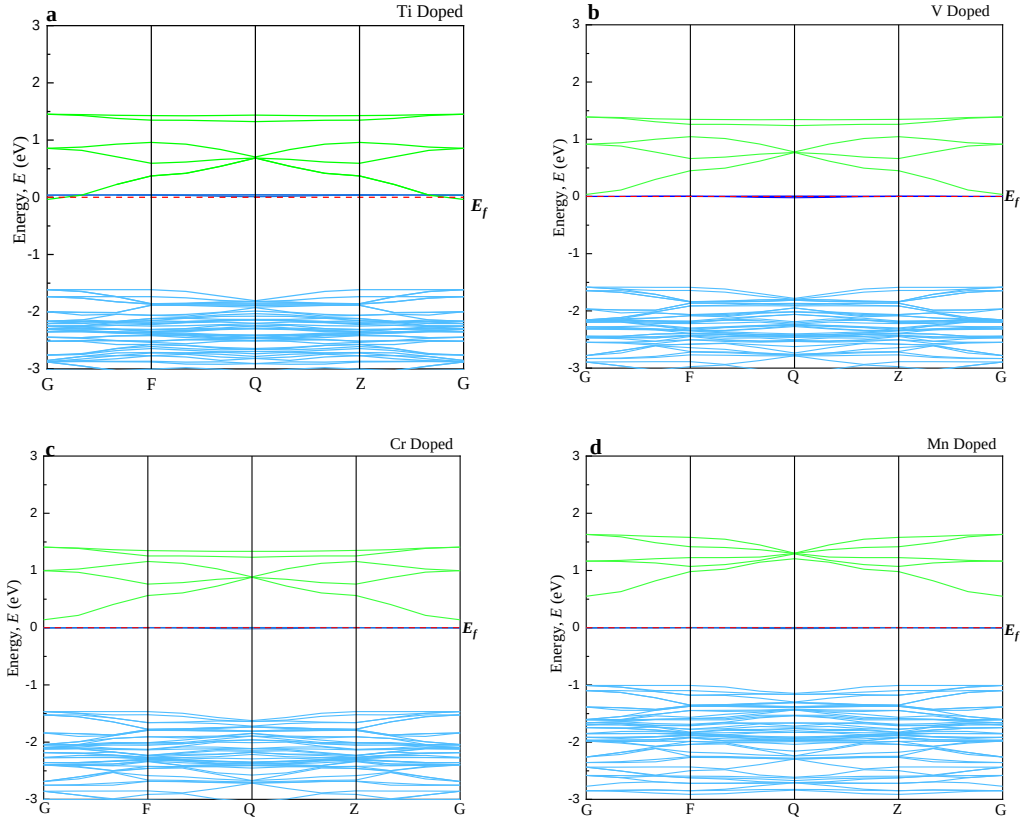

Fig. 4.4: The electronic band structure of $Cs_2NaGaBr_6$ double perovskite for (a) Ti-doped sample, (b) V-doped sample (c) Cr-doped sample, and (d) Mn-doped sample.

The Cr-doped sample shows a similar result to the V-doped sample. It gives a direct band-gap of 1.6 eV and due to the appearance of the intermediate state at the fermi level (E_f), the transfer of electrons becomes easier. From Fig. 4.4(d), it is clear that for the Mn-doped sample, the conduction band shifts towards the higher energy region. However, the peak of the valence band also shifts towards the high energy region and gets close to the fermi level which results in a direct band-gap of 1.55 eV. Again, for the Mn-doped $Cs_2NaGaBr_6$ sample, the appearance of an intermediate state between the band gap at the fermi level makes the transfer of electrons from the valence band to the conduction band much easier. The band gap between this intermediate state and the lower

portion of the conduction band is 0.55 eV. As a result, a high absorption in the lower energy (visible) region is observed for the Mn-doped $Cs_2NaGaBr_6$ sample in Fig. 4.7.

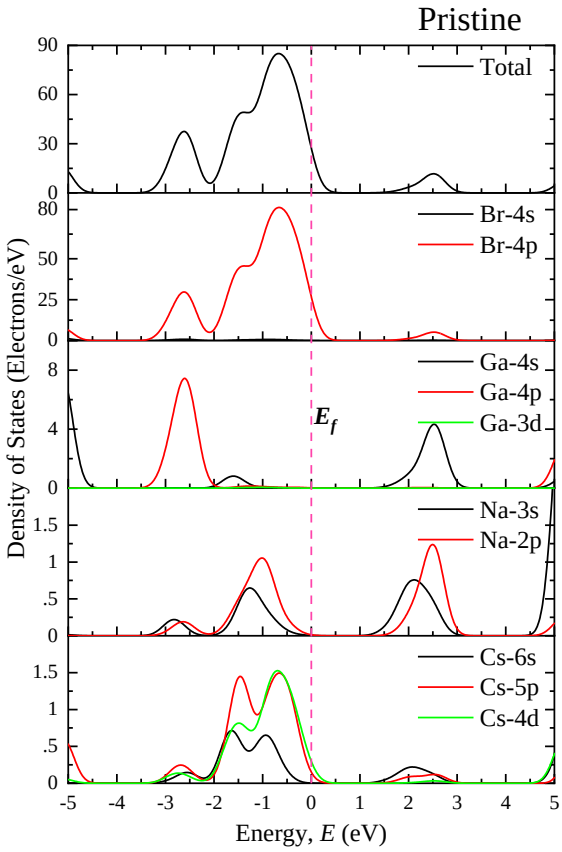

Fig. 4.5: Total and partial DOS of Pristine $Cs_2NaGaBr_6$.

The Fig. 4.5 demonstrates the TDOS (Total Density of State) and PDOS (Partial Density of State) of Pristine $Cs_2NaGaBr_6$. The exhibited valence band (below the E_f) of this figure is mainly composed of Br-4p orbital with little contribution of Cs-4d, Cs-5p, and Ga-4p orbitals. On the other hand, the conduction band which is above the E_f is mostly comprised of Na-2p, Ga-4s, and Br-4p orbitals. This PDOS diagram gives an insight into the band structure by demonstrating the contribution of particular orbitals of each element.

The partial and total density of the state of Ti-doped, V-doped, Cr-doped, and Mn-doped $Cs_2NaGaBr_6$ are illustrated in Fig. 4.6. The graphs show that the valence band shifts toward the low energy level for the doped samples compared to the pristine sample (fig. 4.5). However, the

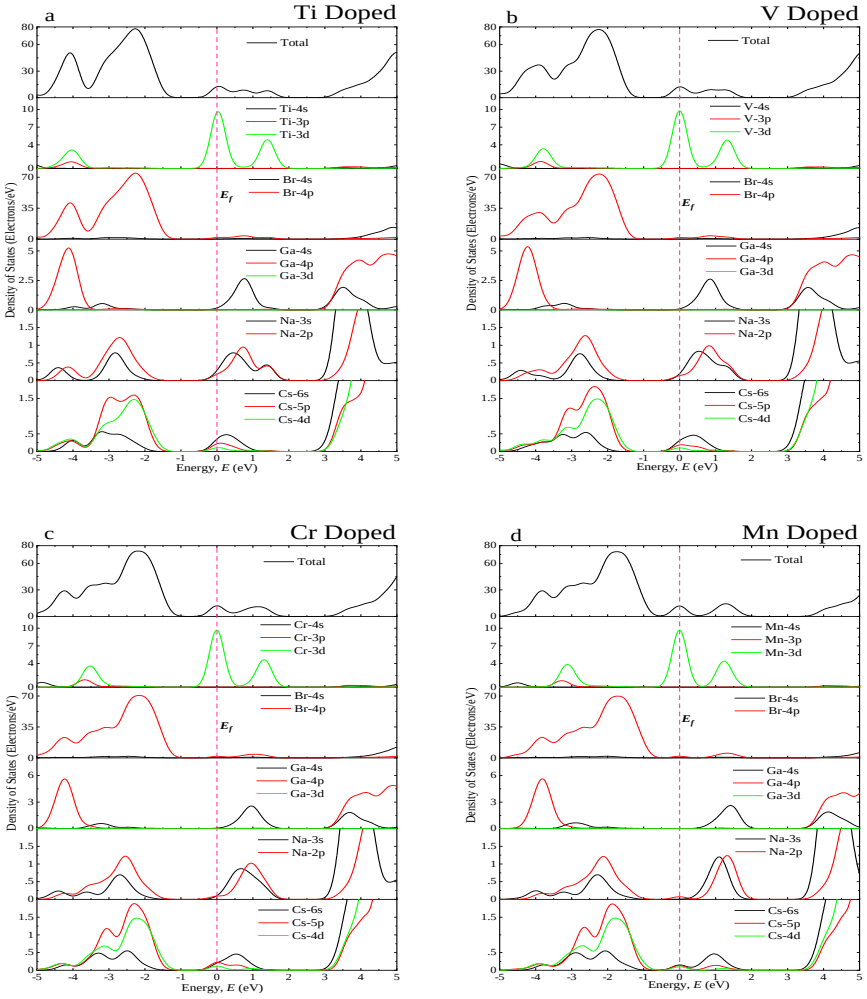

Fig. 4.6: Total and partial DOS of (a) Ti-doped, (b) V-Doped, (c) Cr-doped, and (d) Mn-doped $Cs_2NaGaBr_6$ double perovskite.

conduction bands also shift toward the lower energy region (fig.4.6). Also, in the fermi level (E_f), an extra peak is visible for all the doped samples. This is due to the creation of dopant states Ti-3d, V-3d, Cr-3d, and Mn-3d for Ti-doped, V-doped, Cr-doped, and Mn-doped samples respectively.

From the fig. 4.6, it is visible that the dopant states have changed the band-gap by contributing near and at the fermi level. For all the doped samples of $Cs_2NaGaBr_6$, the dopant energy states

have appeared between the band gaps. Here, the process of transferring valence electrons to the conduction band is facilitated by the presence of intermediate energy states introduced by the dopants. Initially, these electrons move from the valence band to the intermediate band, created by the dopant's energy levels. Then, under the visible light energy, they progress to the conduction band. This mechanism is vital as it requires less energy for the transfer of excited photoelectrons. The presence of these intermediate states leads to a red-shift and an increase in the light absorption capabilities of the metal-doped $Cs_2NaGaBr_6$ samples, compared to the pristine $Cs_2NaGaBr_6$.

4.1.3 Optical Properties

Understanding the optical functions of a substance is crucial in various scientific and technological fields, including photovoltaic devices, materials science, and engineering. The electronic configuration depends on the optical properties of materials used in solar cells. The lead-free and halide double perovskite $Cs_2NaGaBr_6$ shows good results for solar cell materials possessing high optical absorption and optical conductivity [12]. So, for potential optoelectronic device application, the optical properties including the optical absorption, the optical conductivity, the real and imaginary part of dielectric functions, and the optical reflectivity of pristine and metal-doped (Ti, V Cr, Mn) $Cs_2NaGaBr_6$ are investigated in this study. The fig. 4.7 highlights the optical absorption spectra of the pristine and metal-doped $Cs_2NaGaBr_6$. In the context of optics, absorption occurs when photons of light are absorbed by the electrons in the atoms or molecules of a material.

Different materials have unique absorption spectra, which describe the wavelengths of light that are absorbed most efficiently by the material. The absorption spectrum provides information about the energy levels of the material and the electronic transitions it undergoes. The absorption coefficient quantifies the reduction in intensity of the light as it passes through per unit length of the material. In other words, the absorption coefficient provides information about how effectively a material absorbs the energy of incident light. It is a crucial parameter in understanding the interaction between incident light and the material and hence provides valuable information about the material’s capability in building solar cell devices. Fig. 4.7(a) illustrates the photon energy-dependent absorption spectra of pristine and doped $Cs_2NaGaBr_6$. From the figure, it is clear that the doped samples show better absorption at the visible region (1.63 eV to 3.26 eV) compared to the pristine sample. The Ti-doped and Mn-doped samples show a significant shift towards the low

photon energy zone (redshift) compared with the pristine sample. Both Ti-doped and Mn-doped samples exhibit the high absorption peak that is noticed at ~ 3 eV. Following that, the pristine, V-doped, and Cr-doped samples showed their absorption peak around the same energy region. However, the energy coefficient enhanced largely in the visible region for the doped samples. The absorption nature of all the doped and pristine samples is approximately similar. however, the peak absorption coefficient for Ti-doped sample is ~ 1.6×10^4 cm^{-1} which is significantly higher than the pristine $Cs_2NaGaBr_6$ which is ~ 8.2×10^3 cm^{-1}. This gives great insights regarding absorption for the doping samples. The absorption coefficient is enhanced on a larger scale in the low-energy region due to the metal doping. For a better understanding of the light absorption in the visible region, fig. 4.7(b) demonstrates the absorption coefficient as a function of wavelength from 300 nm to 800 nm. The metal-doped double $Cs_2NaGaBr_6$ perovskites reveal higher absorption in the visible wavelength compared to the pristine $Cs_2NaGaBr_6$. For all the solar energy that arrives on the earth, about 43% of that solar spectrum is light energy [37]. Therefore, the metal-doped double perovskite samples show more capability to utilize visible light of the solar spectrum than the pristine sample of $Cs_2NaGaBr_6$. Hence, doped samples are significantly better for solar cell fabrication than the pristine sample. Among them, the Ti-doped and Mn-doped samples show the most potential due to their very high absorption coefficient in the visible range. Therefore, the metal-doped double perovskite can be a potential candidate for the fabrication of solar cells.

Optical conductivity is a measure of how well a material conducts electric current in response to the absorption of light. It is specified as photoconductivity. The increase in photoconductivity occurs due to the increased absorption of photons. The real part of the conductivity spectra is shown in Fig. 4.8(a). The range is from 0 eV to 20 eV photon energy for pristine and all metal-doped $Cs_2NaGaBr_6$ samples. In the high-energy region, the pristine sample shows higher conductivity than the doped samples. However, in the low energy region (visible), metal-doped $Cs_2NaGaBr_6$ samples have higher conductivity. In the low energy region, a sharp peak is observed for the Ti-doped $Cs_2NaGaBr_6$. V, Cr, and Mn-doped samples also show peaks around the visible low-energy region (1.63 eV to 3.26 eV). These results are the reflection of the high absorption of metal-doped samples in the visible region demonstrated in Fig. 4.7(a). Reflectivity is a crucial consideration in the design and efficiency of solar cells and photovoltaic devices. The reflectivity of a material refers to its ability to reflect light or other electromagnetic waves. It is a measure of how much incident light is reflected from the surface of the material. Fig. 4.8(b) illustrates the

reflectivity spectra of pristine and metal-doped $Cs_2NaGaBr_6$ for light energy. From the figure, it is clear that the pristine sample of $Cs_2NaGaBr_6$ shows the lowest reflectivity in the visible low-energy region. Whereas, the metal-doped samples reveal high reflectivity over the whole solar spectrum. For better absorption and performance of the optoelectronic devices, further studies should be carried out in order to reduce the reflectivity of the metal-doped $Cs_2NaGaBr_6$ samples.

The dielectric function is a key parameter in the study of the optical properties of materials. It describes how a material responds to an external field, particularly in the context of electromagnetic waves, such as light. The dielectric function is a complex quantity having both real and imaginary parts. It is fundamental in describing how materials interact with light. It influences the reflection, transmission, and absorption of electromagnetic waves in different materials. The way a material reacts to incident photon energy can be described by the dielectric function.

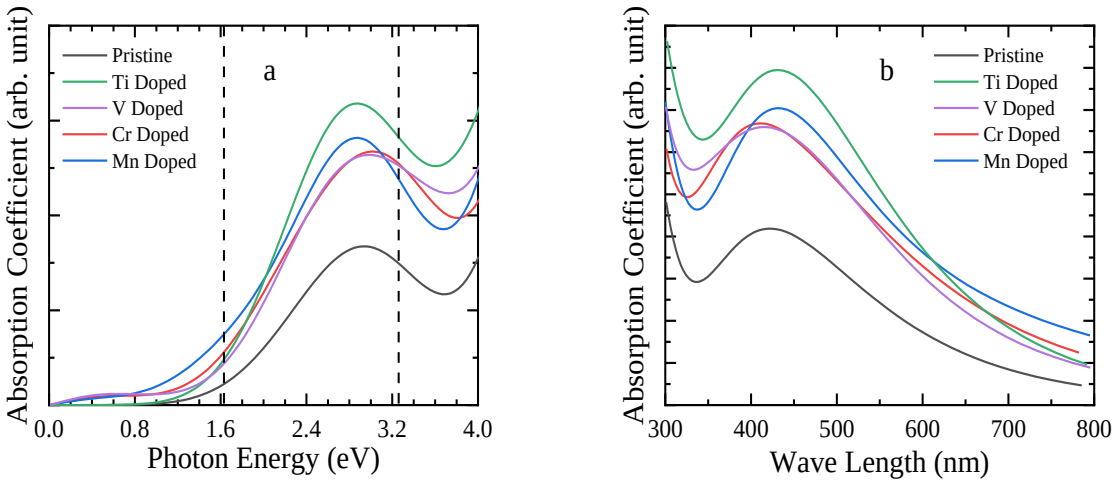

Fig. 4.7: Light absorption spectra of pristine and metal-doped $Cs_2NaGaBr_6$ materials, (a) absorption coefficient as a function of light energy and (b) as a function of the wavelength of light.

The static value of the dielectric constant is a valuable indicator that offers significant insights into the rate of charge recombination which affects the overall efficiency of optoelectronic devices [38] A material with a high dielectric constant indicates a relatively low rate of charge carrier

recombination. Consequently, this leads to an enhancement in the overall performance of optoelectronic devices.

Fig. 4.9(a) and fig. 4.9(b) displays the real and imaginary parts of the dielectric function of pristine and doped samples of $Cs_2NaGaBr_6$ respectively. The figure exhibits a sharp peak for the metal-doped $Cs_2NaGaBr_6$ samples in the both real and imaginary parts of the low-energy region. The Ti and Mn-doped samples show the highest peak in the lower energy region. On the other hand, the pristine sample reveals a comparatively low value of dielectric function to that of metal-doped samples. Generally, materials with a wide value of band gap show a lower value of dielectric constant [39].

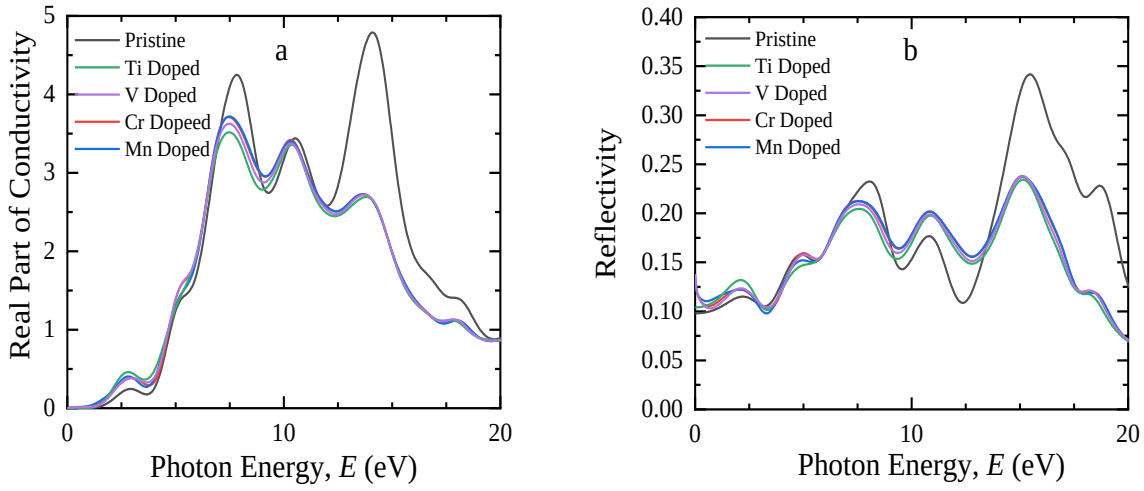

Fig. 4.8: Calculated spectra of (a) optical conductivity, and (b) reflectivity of pristine and metal-doped $Cs_2NaGaBr_6$ samples as a function of photon energy.

The electronic properties reveal the reduction of bandgap due to the appearance of intermediate states after the metal doping into the double perovskite $Cs_2NaGaBr_6$. Therefore, the metal-doped samples exhibit a higher value of dielectric function than the pristine $Cs_2NaGaBr_6$ sample. The electronic band structure of a crystal is directly connected to the imaginary part of the dielectric function and it also describes the absorption behaviour of material [40]. The emergence of a noticeable peak in the imaginary part of the dielectric function for metal-doped $Cs_2NaGaBr_6$ materials in the visible range indicates that the doped samples exhibit significant absorbance in that region, which is supported by the absorption spectra. Moreover, the metal-doped $Cs_2NaGaBr_6$

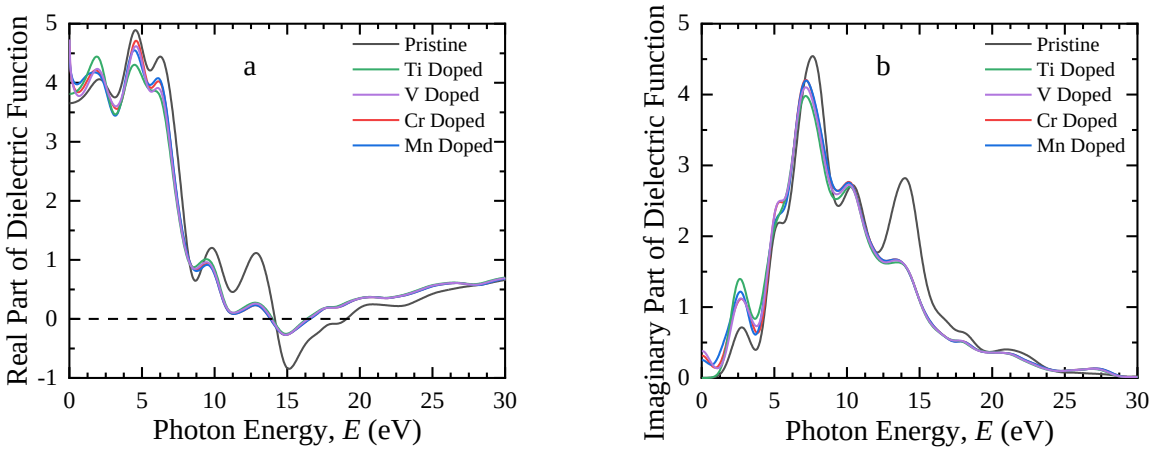

Fig. 4.9: Dielectric function (a) real part, and (b) imaginary part of pristine and metal-doped $Cs_2NaGaBr_6$ samples as a function of photon energy.

samples demonstrate high dielectric function values in the low-energy range, suggesting their potential as promising candidates for use in optoelectronic applications. Near the high energy region (30 eV), the imaginary part of the dielectric function of all the samples reaches zero and the real part goes to unitary. These results suggest that both pristine and doped $Cs_2NaGaBr_6$ show higher absorption in the low-energy (visible) region compared to the high-energy region.

Chapter 5

Conclusions

5.1 Summary of the Thesis

In the study, the effect of metal doping on the structural, electrical, and optical properties of $Cs_2NaGaBr_6$ has been examined by first-principles calculations based on density functional theory (DFT).

The core findings of the thesis are summarised below:

- The existing pristine $Cs_2NaGaBr_6$ is not fully efficient for efficient utilization of the solar spectrum in photovoltaic conversion. Strategically incorporating metal doping can considerably improve both the absorption of light and the conductivity of electricity.
- The addition of Titanium (Ti) and Manganese (Mn) has been discovered to significantly increase the absorbance and photoconductivity of $Cs_2NaGaBr_6$ in comparison to its original state. Significantly, both Ti- and Mn-doped $Cs_2NaGaBr_6$ samples exhibit the highest absorption peak at 3 eV, precisely located inside the visible spectrum.
- The pristine $Cs_2NaGaBr_6$ has a low level of reflectivity throughout the entire range of the solar energy spectrum. However, the metal-doped versions show significantly higher reflectivity. This factor is a crucial aspect to consider for prospective implementations in the absorption of solar energy.
- The doping of metals into $Cs_2NaGaBr_6$ resulted in significant improvements in its dielectric characteristics. Both real and imaginary parts of the dielectric function display a distinct peak in the low energy range, which is significantly different from the lower values (>1) observed for the pristine sample. More precisely, the highest value of the real part of the dielectric function is observed at 1.87 eV for the Ti-doped sample.
- The highest peak in the imaginary part of the dielectric function near 2.6 eV within the visible range for the metal-doped materials demonstrates a strong correlation with their elevated absorbance levels, as seen by the absorption spectra. The increased dielectric

function at low energies strongly indicates that the metal-doped $Cs_2NaGaBr_6$ are highly promising options for optoelectronic device applications, presenting substantial enhancements compared to the pristine material.

- The metal doping is crucial in tailoring the band structure of $Cs_2NaGaBr_6$, which leads to improvements in its optoelectronic characteristics. Transition metals are added to $Cs_2NaGaBr_6$ to provide additional energy levels in its band structure. These additional states efficiently reduce the width of the energy gap by introducing intermediate states, bringing it into closer alignment with the energy distribution of solar radiation. The alignment is essential because it enhances the absorption of solar photons, especially in the visible range of the spectrum, resulting in improved efficiency.
- The tailored band structure resulting from metal doping not only increases light absorption but also impacts the electronic transitions within the material. This leads to more efficient separation and transport of photon-generated charge carriers. This is a crucial element for achieving high-performance photovoltaic uses. Hence, the manipulation of the band structure by metal doping plays a crucial role in fully exploring the optoelectronic capabilities of $Cs_2NaGaBr_6$ for solar cell applications.

5.2 Future Works

For future research, the following areas are recommended for exploration:

- Using advanced computational methods such as DFT+U in DFT for the calculation in order to get better and more precious theoretical outcome.
- Analyzing the mechanical property of doped $Cs_2NaGaBr_6$ samples. This will give a better idea on the stability of the material.
- Analyzing the physical properties of doped $Cs_2NaGaBr_6$ samples under various pressures and different concentrations.
- Experimental research in order to analyze the physical properties of doped $Cs_2NaGaBr_6$ and verify the theoretical predictions.

References

[1] P. L. ' 'Taylor and O. 'Heinonen, *A Quantum Approach to Condensed Matter Physics*. Cambridge University Press, UK, 2002.

[2] H. J. Snaith, "Perovskites: The emergence of a new era for low-cost, high-efficiency solar cells," *Journal of Physical Chemistry Letters*, vol. 4, no. 21. pp. 3623–3630, Nov. 07, 2013. doi: 10.1021/jz4020162.

[3] Z. Wang, A. M. Ganose, C. Niu, and D. O. Scanlon, "First-principles insights into tin-based two-dimensional hybrid halide perovskites for photovoltaics," *J Mater Chem A Mater*, vol. 6, no. 14, pp. 5652–5660, Apr. 2018, doi: 10.1039/c8ta00751a.

[4] R. F. Service, "Energy technology: Perovskite solar cells keep on surging," *Science*, vol. 344, no. 6183. American Association for the Advancement of Science, p. 458, 2014. doi: 10.1126/science.344.6183.458.

[5] A. Kojima, K. Teshima, Y. Shirai, and T. Miyasaka, "Organometal halide perovskites as visible-light sensitizers for photovoltaic cells," *J Am Chem Soc*, vol. 131, no. 17, pp. 6050–6051, May 2009, doi: 10.1021/ja809598r.

[6] N. G. Park, "Organometal perovskite light absorbers toward a 20% efficiency low-cost solid-state mesoscopic solar cell," *Journal of Physical Chemistry Letters*, vol. 4, no. 15, pp. 2423–2429, Aug. 2013, doi: 10.1021/jz400892a.

[7] A. Walsh, "Principles of chemical bonding and band gap engineering in hybrid organic-inorganic halide perovskites," *Journal of Physical Chemistry C*, vol. 119, no. 11, pp. 5755–5760, Mar. 2015, doi: 10.1021/jp512420b.

[8] R. Fu *et al.*, "Pressure-induced structural transition and band gap evolution of double perovskite Cs2AgBiBr6 nanocrystals," *Nanoscale*, vol. 11, no. 36, pp. 17004–17009, Sep. 2019, doi: 10.1039/c9nr07030c.

[9] G. García-Espejo, D. Rodríguez-Padrón, R. Luque, L. Camacho, and G. De Miguel, "Mechanochemical synthesis of three double perovskites: Cs2AgBiBr6,

(CH3NH3)2TlBiBr6 and Cs2AgSbBr6," *Nanoscale*, vol. 11, no. 35, pp. 16650–16657, Sep. 2019, doi: 10.1039/c9nr06092h.

[10] L. Schade *et al.*, "Structural and Optical Properties of Cs 2 AgBiBr 6 Double Perovskite," *ACS Energy Lett*, vol. 4, no. 1, pp. 299–305, Jan. 2019, doi: 10.1021/acsenergylett.8b02090.

[11] Z. Zhang, Z. Wu, D. Rincon, C. Garcia, and P. D. Christofides, "Operational safety of chemical processes via Safeness-Index based MPC: Two large-scale case studies," *Comput Chem Eng*, vol. 125, pp. 204–215, Jun. 2019, doi: 10.1016/j.compchemeng.2019.03.003.

[12] Y. Saeed *et al.*, "$Cs_2NaGaBr_6$: A new lead-free and direct band gap halide double perovskite," *RSC Adv*, vol. 10, no. 30, pp. 17444–17451, May 2020, doi: 10.1039/d0ra01764g.

[13] A. Menedjhi, N. Bouarissa, S. Saib, and K. Bouamama, "Halide double perovskite Cs2AgInBr6 for photovoltaic's applications: Optical properties and stability," *Optik (Stuttg)*, vol. 243, Oct. 2021, doi: 10.1016/j.ijleo.2021.167198.

[14] A. Kumar, M. S. Thomas, N. Gupta, A. K. Goyal, and Y. Massoud, "Enhanced Photovoltaic Assessment of Pb-Free $Cs_2NaGaBr_6$ n-i-p Solar Cell by ETL Optimizations," in *Proceedings of the IEEE Conference on Nanotechnology*, IEEE Computer Society, 2023, pp. 1002–1005. doi: 10.1109/NANO58406.2023.10231198.

[15] Y. Zhou, J. Chen, O. M. Bakr, and H. T. Sun, "Metal-Doped Lead Halide Perovskites: Synthesis, Properties, and Optoelectronic Applications," *Chemistry of Materials*, vol. 30, no. 19. American Chemical Society, pp. 6589–6613, Oct. 09, 2018. doi: 10.1021/acs.chemmater.8b02989.

[16] M. N. Islam, M. A. Hadi, and J. Podder, "Influence of Ni doping in a lead-halide and a lead-free halide perovskites for optoelectronic applications," *AIP Adv*, vol. 9, no. 12, Dec. 2019, doi: 10.1063/1.5132985.

[17] J. Islam and A. K. M. A. Hossain, "Narrowing band gap and enhanced visible-light absorption of metal-doped non-toxic CsSnCl3 metal halides for potential optoelectronic applications," *RSC Adv*, vol. 10, no. 13, pp. 7817–7827, Feb. 2020, doi: 10.1039/c9ra10407k.

[18] M. T. Project, “Materials Data on $Cs_2NaGaBr_6$ by Materials Project,” 2020.

[19] M. D. Segall *et al.*, “First-principles simulation: ideas, illustrations and the CASTEP code,” 2002.

[20] D. Vanderbilt, “Rapid Communications Soft self-consistent pseudopotentials in a generalized eigenvalue formalism.”

[21] J. P. Perdew, K. Burke, and M. Ernzerhof, “Generalized Gradient Approximation Made Simple,” 1996.

[22] H. J. Monkhorst and J. D. Pack, “Special points for Brillonin-zone integrations*,” 1976.

[23] D. C. Liu and J. Nocedal, “ON THE LIMITED M E M O R Y BFGS M E T H O D FOR LARGE SCALE O P T I M I Z A T I O N,” 1989.

[24] C. Ambrosch-Draxl and J. O. Sofo, “Linear optical properties of solids within the full-potential linearized augmented planewave method,” 2004.

[25] P. Y. Yu and M. Cardona, *Fundamentals of semiconductors : physics and materials properties*. Springer, 2010.

[26] A. Delin *et al.*, “Optical properties of the group-IVB refractory metal compounds,” 1996.

[27] L. Kleinman and C. J. Ytn, “Relativistic norm-conserving pseutioyotential 15 MARCH 1980 is’ (for negative and positive «, respectively).”

[28] M. A. Hadi, “First-principles Study of Superconducting MAX Phases.” [Online]. Available: https://www.researchgate.net/publication/299594633

[29] I. E. Gaa, P. Hohenbergt Ecole, X. Superzeure, I’aris, F. And, and W. Konnt, “PHYSICAL REVIEW.”

[30] W. Kohn and L. J. Sham, “PHYSICAL REVIEW Self-Consistent Equations Including Exchange and Correlation Effects*.”

[31] F. W. Kutzler and G. S. Painter, “First-row diatomics: Calculation of the geometry and energetics using self-consistent gradient-functional approximations.”

[32] M. T. Nasir *et al.*, “First-principles study of superconducting ScRhP and ScIrP pnictides.”

[33] E. T. McClure, M. R. Ball, W. Windl, and P. M. Woodward, “Cs2AgBiX6 (X = Br, Cl): New Visible Light Absorbing, Lead-Free Halide Perovskite Semiconductors,” *Chemistry of Materials*, vol. 28, no. 5, pp. 1348–1354, Mar. 2016, doi: 10.1021/acs.chemmater.5b04231.

[34] A. D. Becke, “A new mixing of Hartree-Fock and local density-functional theories,” *J Chem Phys*, vol. 98, no. 2, pp. 1372–1377, 1993, doi: 10.1063/1.464304.

[35] F. Aryasetiawan and O. Gunnarsson, “The GW method,” 1998. [Online]. Available: http://iopscience.iop.org/0034-4885/61/3/002

[36] A. K. Singh, A. Janotti, M. Scheffler, and C. G. Van De Walle, “Sources of electrical conductivity in SnO2,” *Phys Rev Lett*, vol. 101, no. 5, Jul. 2008, doi: 10.1103/PhysRevLett.101.055502.

[37] X. Zong *et al.*, “Activation of photocatalytic water oxidation on N-doped ZnO bundle-like nanoparticles under visible light,” *Journal of Physical Chemistry C*, vol. 117, no. 10, pp. 4937–4942, Mar. 2013, doi: 10.1021/jp311729b.

[38] X. Liu *et al.*, “A high dielectric constant non-fullerene acceptor for efficient bulk-heterojunction organic solar cells,” *J Mater Chem A Mater*, vol. 6, no. 2, pp. 395–403, 2018, doi: 10.1039/c7ta10136h.

[39] M. Roknuzzaman, K. (Ken) Ostrikov, K. Chandula Wasalathilake, C. Yan, H. Wang, and T. Tesfamichael, “Insight into lead-free organic-inorganic hybrid perovskites for photovoltaics and optoelectronics: A first-principles study,” *Org Electron*, vol. 59, pp. 99–106, Aug. 2018, doi: 10.1016/j.orgel.2018.04.051.

[40] Hayatullah, G. Murtaza, S. Muhammad, S. Naeem, M. N. Khalid, and A. Manzar, “Physical properties of CsSnM3 (M = Cl, Br, I): A first principle study,” *Acta Phys Pol A*, vol. 124, no. 1, pp. 102–107, Jul. 2013, doi: 10.12693/APhysPolA.124.102.